Supplementary Tables

Table S1. Column integrated AOD and SSA values used for the LUT construction for each research flight, observed from the nearest AERONET site.

Variables (Acronym)	17 OCT 2020 (Chungnam)	3 NOV 2020 (Jaechon)	5 NOV 2020 (Pohang)	24 NOV 2022 (Chungnam)	25 NOV 2022 (Chungnam)
AOD (440 nm)	0.18	0.09	0.21	0.35	0.28
SSA (440 nm)	0.925	0.96	0.96	0.937	0.944
AERONET site (Lat, Lon)	Anmyon (36.539N, 126.330E)	Gangneung_WNU (37.771N, 128.867E)	Gangneung_WNU (37.771N, 128.867E)	Anmyon (36.539N, 126.330E)	Anmyon (36.539N, 126.330E)

Table S2. Reference conditions for the sensitivity test per research flights

Variables (Acronym)	17 OCT 2020 (Chungnam)	3 NOV 2020 (Jaechon)	5 NOV 2020 (Pohang)	24 NOV 2022 (Chungnam)	25 NOV 2022 (Chungnam)
NO_2 VCD	1.00 DU	1.00 DU	1.00 DU	1.00 DU	1.00 DU
PBLH	1.0 km	1.0 km	1.0 km	1.0 km	1.0 km
ALB	0.15	0.15	0.15	0.15	0.15
SZA	48 °	54 °	54 °	57 °	57 °
ALT	1,600 m	1,600 m	2,900 m	1,500 m	1,700 m
VZA	0 °	0 °	0 °	0 °	0 °
RAA	0 °	0 °	0 °	0 °	0 °

Table S3. Details of research flight for the airborne HIS observation. (See Fig. 4 for the acronyms of industrial NO_2 point sources)

Date	Target domain	Potential emission point sources	Airplane type
17 October 2020	Chungnam	PP, PC, SY	Cessna 208
3 November 2020	Jaechon	CK	Cessna 208
5 November 2020	Pohang	SY	Cessna 208
24 November 2022	Chungnam	PP, PC, SY	Beechcraft 1900D
25 November 2022	Chungnam	PP, PC, SY	Beechcraft 1900D

Supplementary Figures

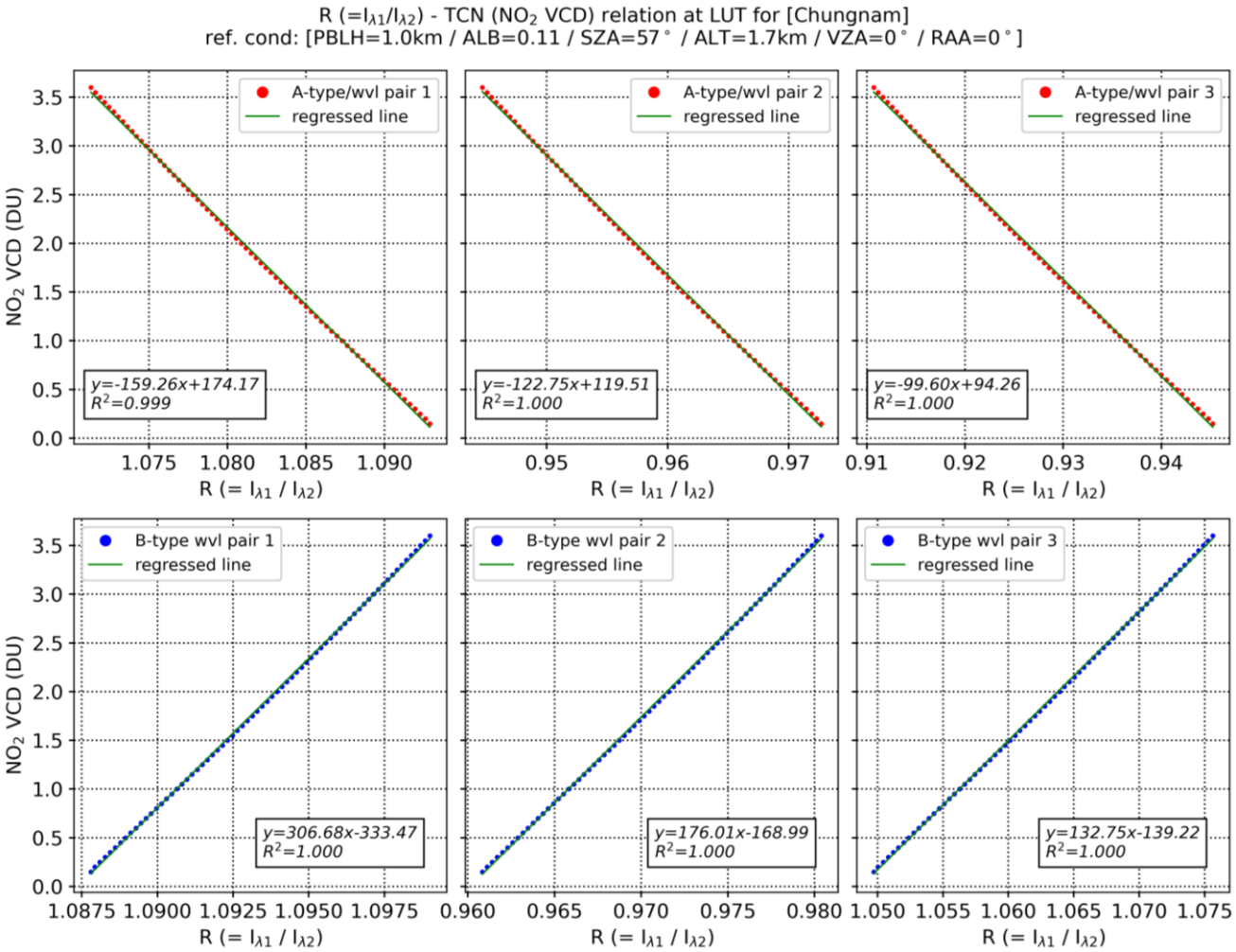

Figure S1. Relationship between R values of the wavelength pairs and the NO_2 VCDs based on forward RTM simulations.

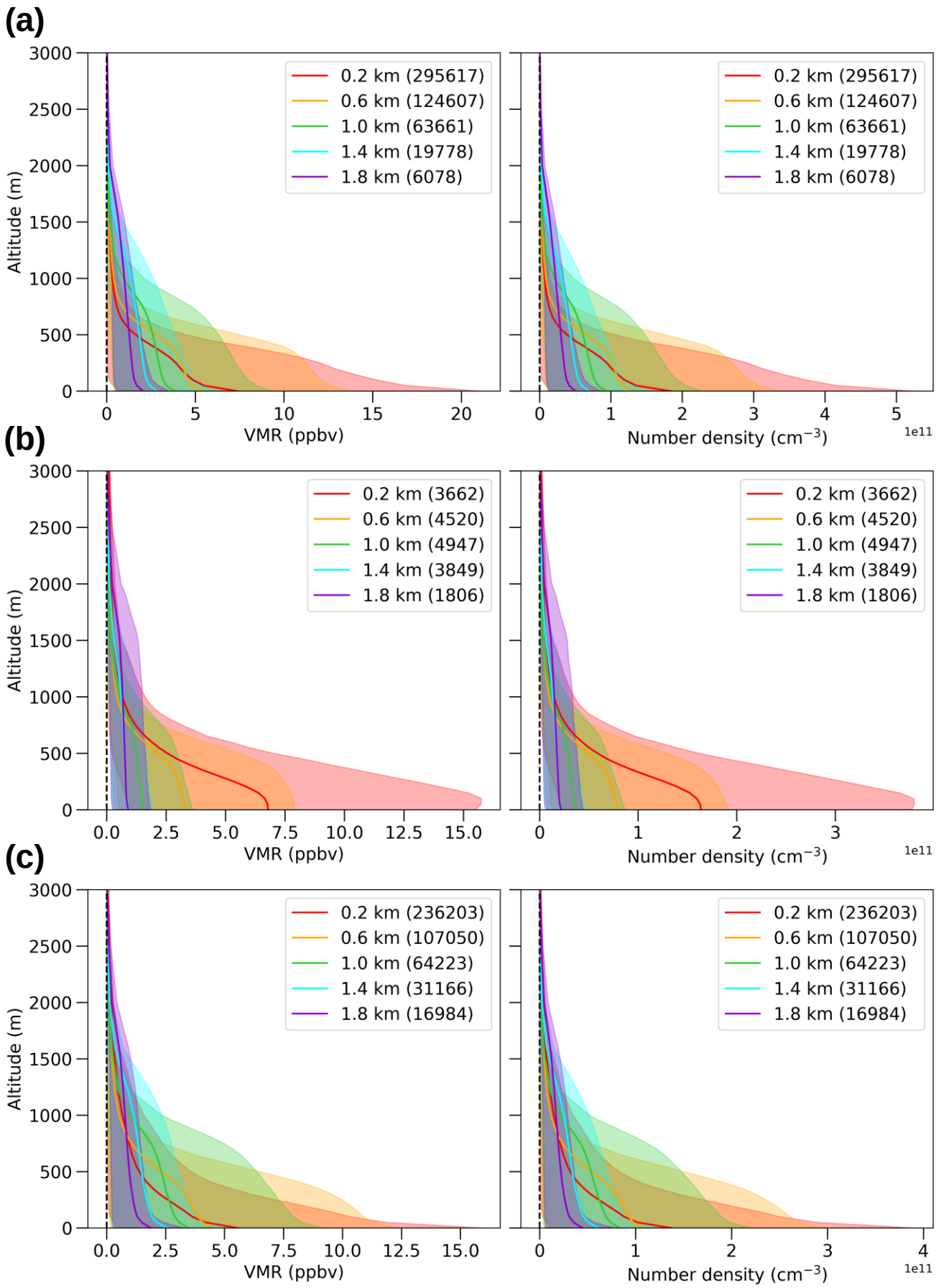

Figure S2. CMAQ-driven vertical profiles of NO_2 volume mixing ratio (left) and number densities (right) at (a) Chungnam, (b) Jaechon, and (c) Pohang domain according to the PBLH. The shaded area shows the 10th and 90th percentiles of NO_2 concentrations at each altitude per PBLH conditions, and the numbers in parentheses are the corresponding vertical profiles accounted for the analysis.

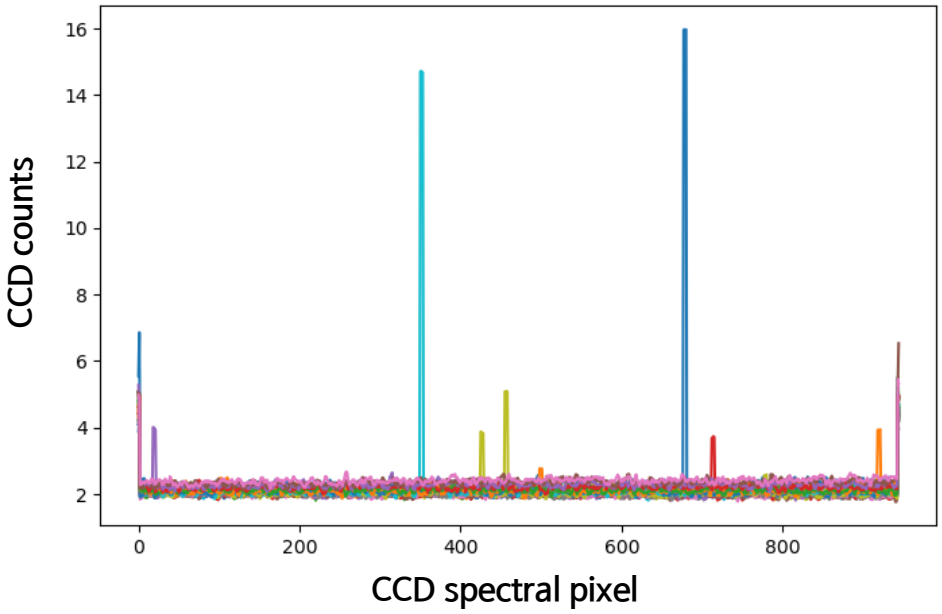

Figure S3. Random noise level per pre-binned spatial pixels (binning 50 raw spatial CCD columns; shown in different colors) under integrated exposure time of 1 second.

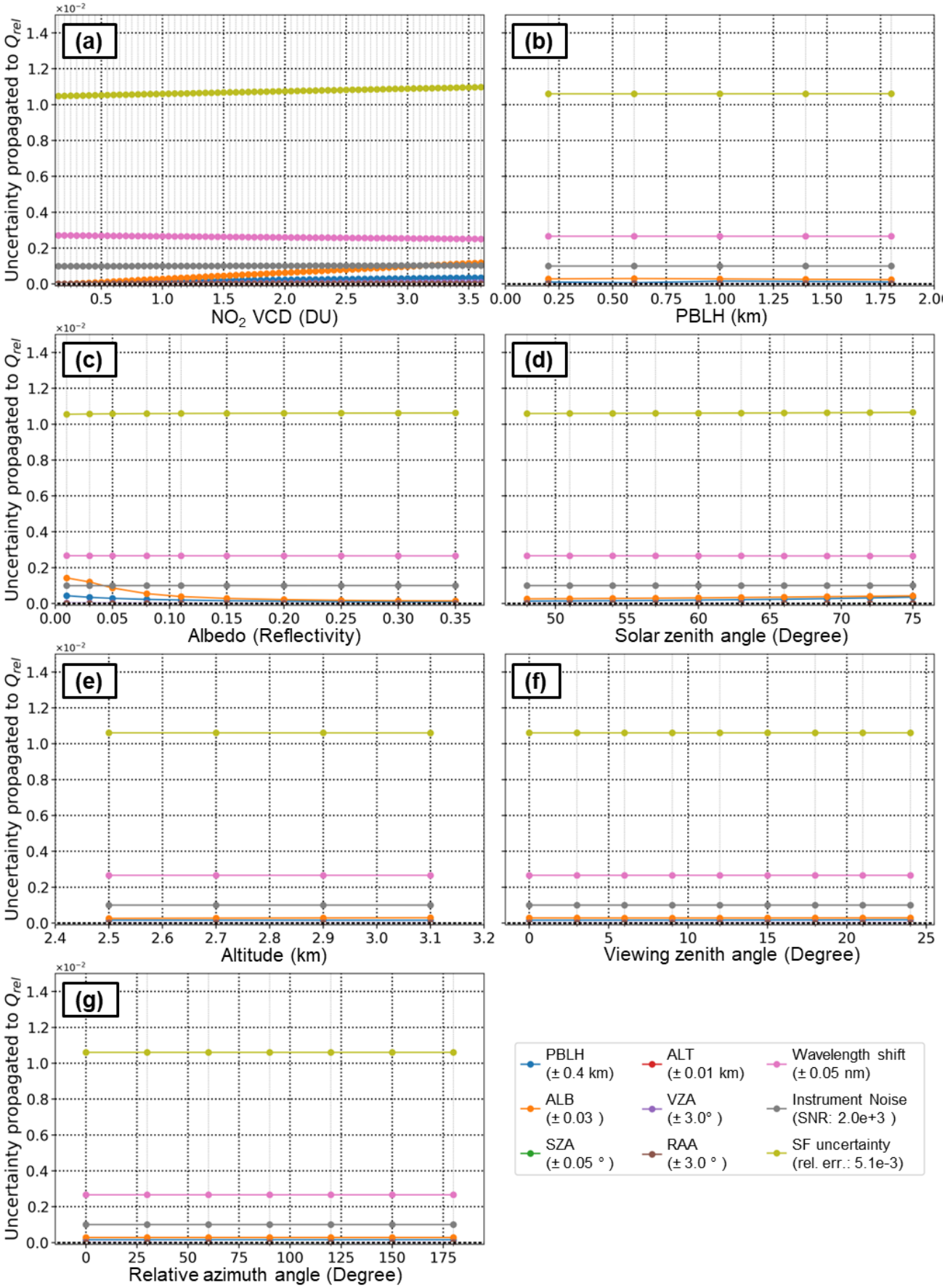

Figure S4. Sensitivity of Q-value calculated from simulated radiances at wavelength-pair 2 (i.e., Type_A: 435.689, 437.015 nm; Type_B: 433.037, 434.363 nm) depending on (a) NO_2 VCD, (b) PBLH, (c) albedo (ALB; reflectivity), (d) solar zenith angle (SZA), (e) observation altitude (ALT), (f) viewing zenith angle (VZA), and (g) relative azimuth angle (RAA) considering atmospheric condition at Pohang and its corresponding reference conditions (shown in supplementary Table S2).

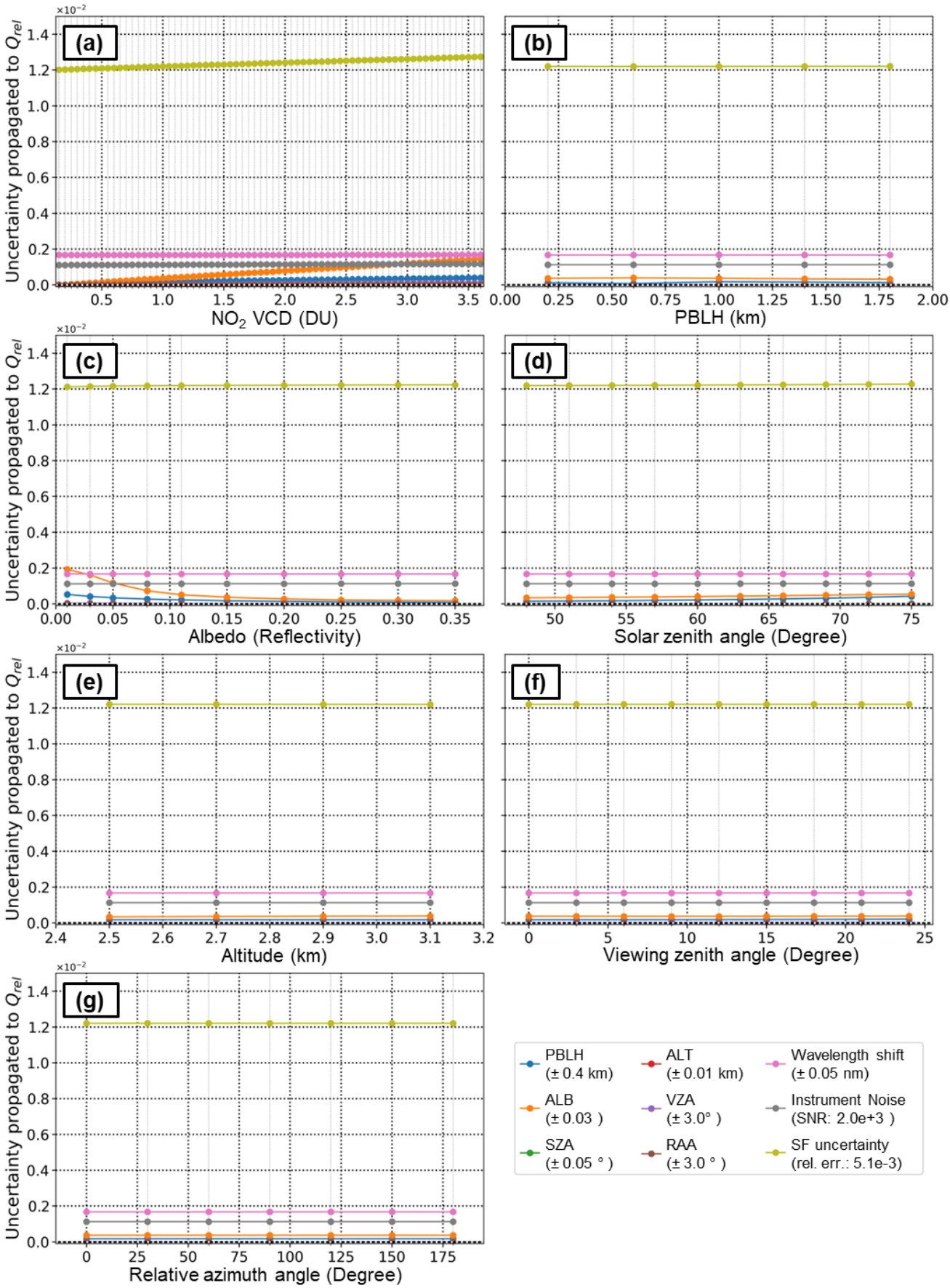

Figure S5. Sensitivity of Q-value calculated from simulated radiances at wavelength-pair 3 (i.e., Type_A: 439.932, 441.258 nm; Type_B: 442.849, 444.175 nm) depending on (a) NO_2 VCD, (b) PBLH, (c) albedo (ALB; reflectivity), (d) solar zenith angle (SZA), (e) observation altitude (ALT), (f) viewing zenith angle (VZA), and (g) relative azimuth angle (RAA) considering atmospheric condition at Pohang and its corresponding reference conditions (shown in supplementary Table S2).

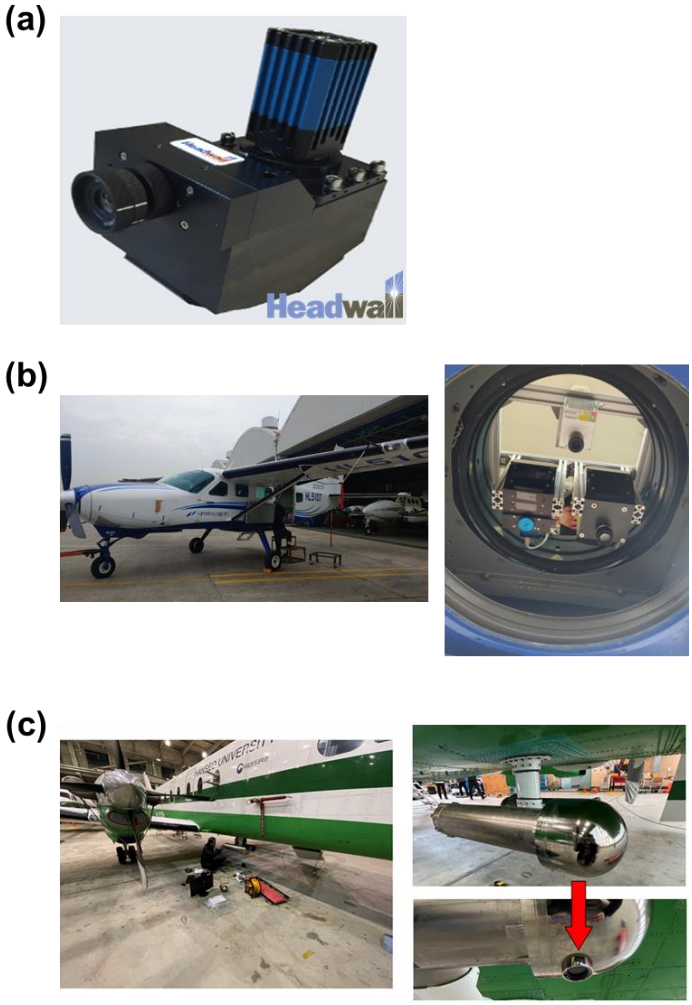

Figure S6. (a) The hyperspectral imaging sensor (HIS), manufactured by Headwall Photonics, Inc., used in this study. (b) Cessna 208 Caravan aircraft (left) and the HIS mounted configure on the camera hole of Cessna plane (right), and (c) Beechcraft 1900D (right) and the HIS mounted on an external canister on a pylon beneath an aircraft (left).

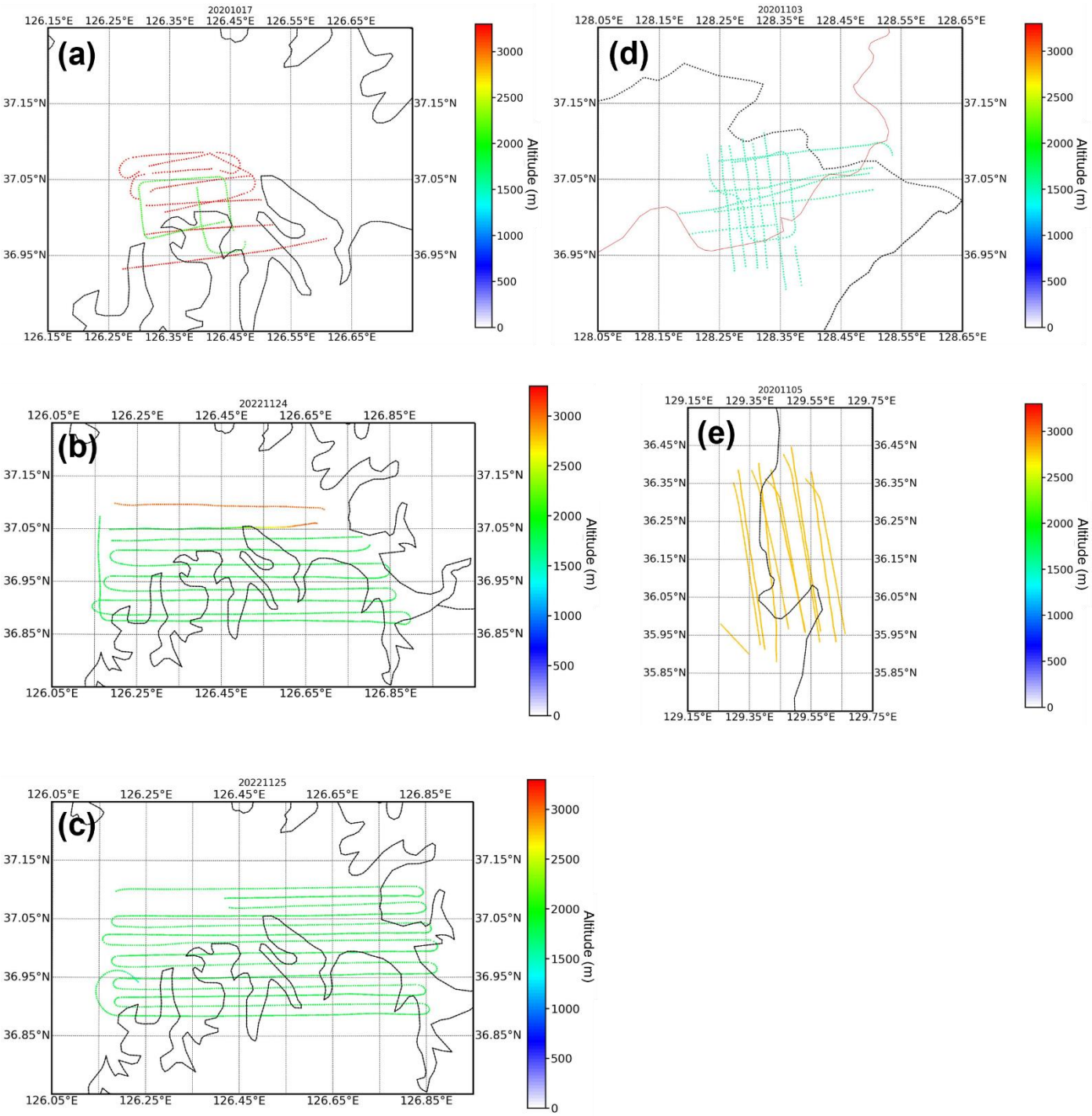

Figure S7. Routes and altitudes of research flights at Chungnam (a-c), Jecheon (d), and Pohang (e) area. Flight dates are shown at the top of each figure.

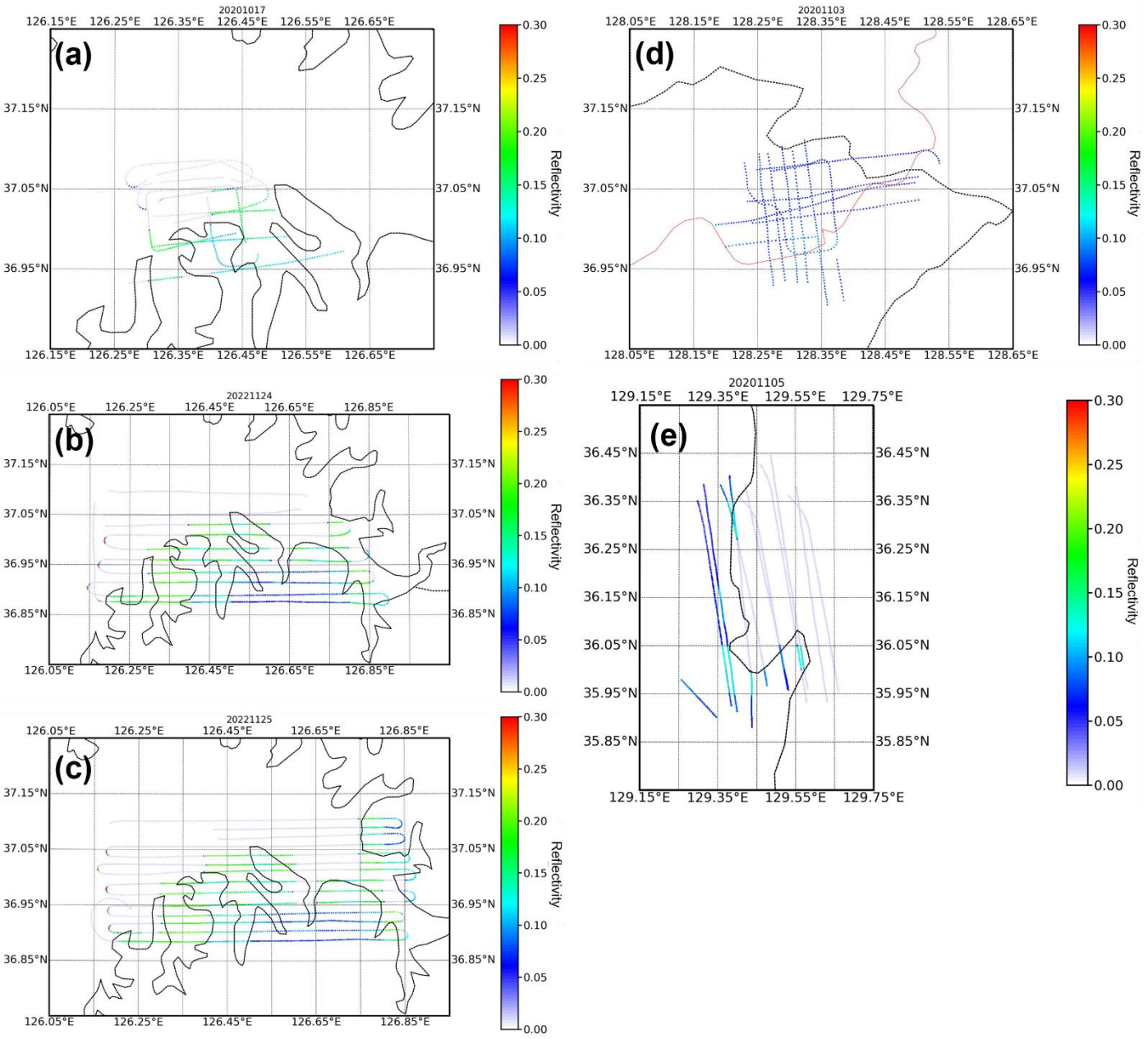

Figure S8. Effective Albedo calculated from VIIRS BRDF kernel and the HIS observation geometry along the research flight track conducted at Chungnam (a-c), Jaechon (d), and Pohang (e) area. Flight dates are shown at the top of each figure.

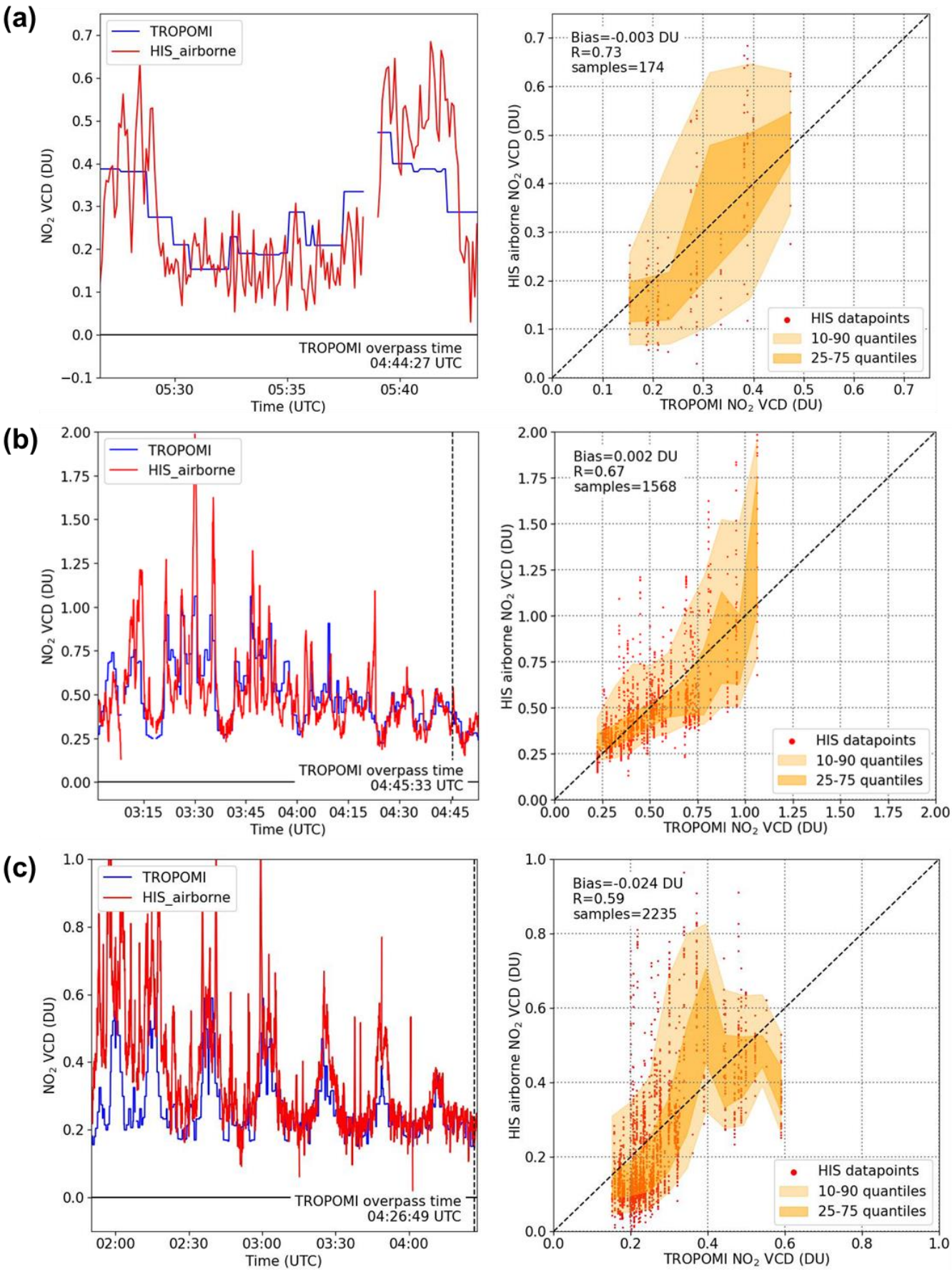

Figure S9. Time series of NO_2 VCD measured from HIS (red line) and TROPOMI (blue line) with TROPOMI overpass time shown in vertical dashed line (left) and the scatter plot comparing the HIS and TROPOMI NO_2 VCDs with the corresponding HIS NO_2 VCD quantiles (10, 25, 75, 90th) shown over the TROPOMI NO_2 VCD range (right) for the research flight at (a) 17 October 2020, (b) 24 November 2022, and (c) 25 November 2022 over the Chungnam domain.

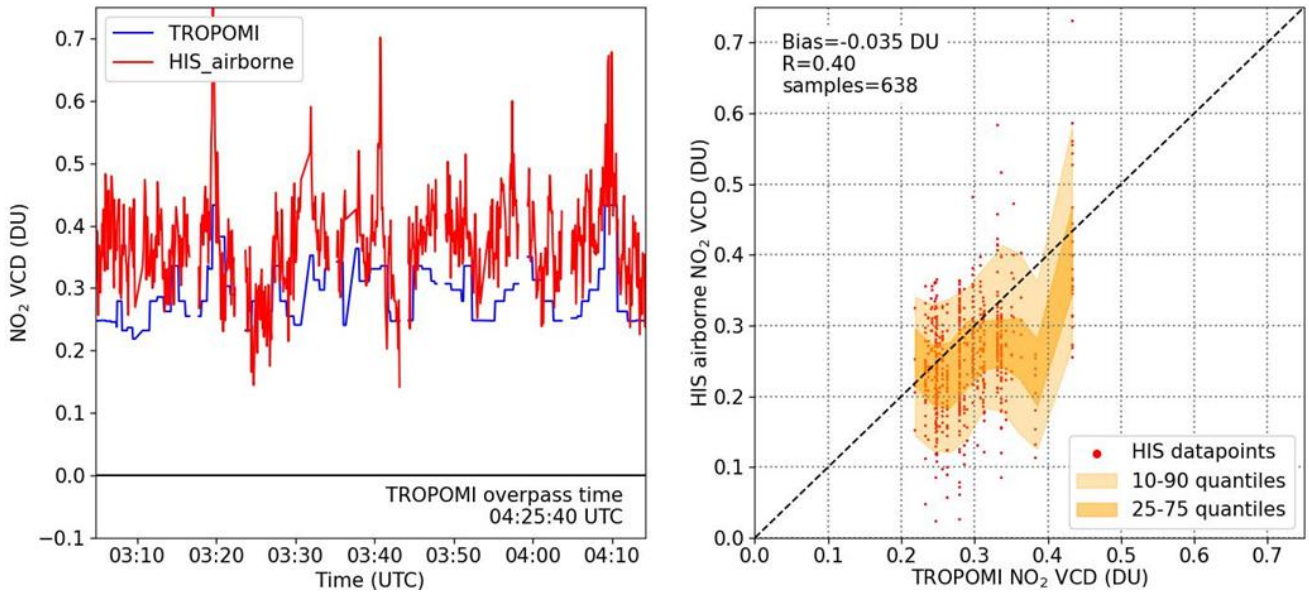

Figure S10. Time series of NO_2 VCD measured from HIS (red line) and TROPOMI (blue line) with TROPOMI overpass time denoted (left) and the scatter plot comparing the HIS and TROPOMI NO_2 VCDs with the corresponding HIS NO_2 VCD quantiles (10, 25, 75, 90th) shown over the TROPOMI NO_2 VCD range (right) for the research flight on 3 November 2020 over the Jaechon domain.

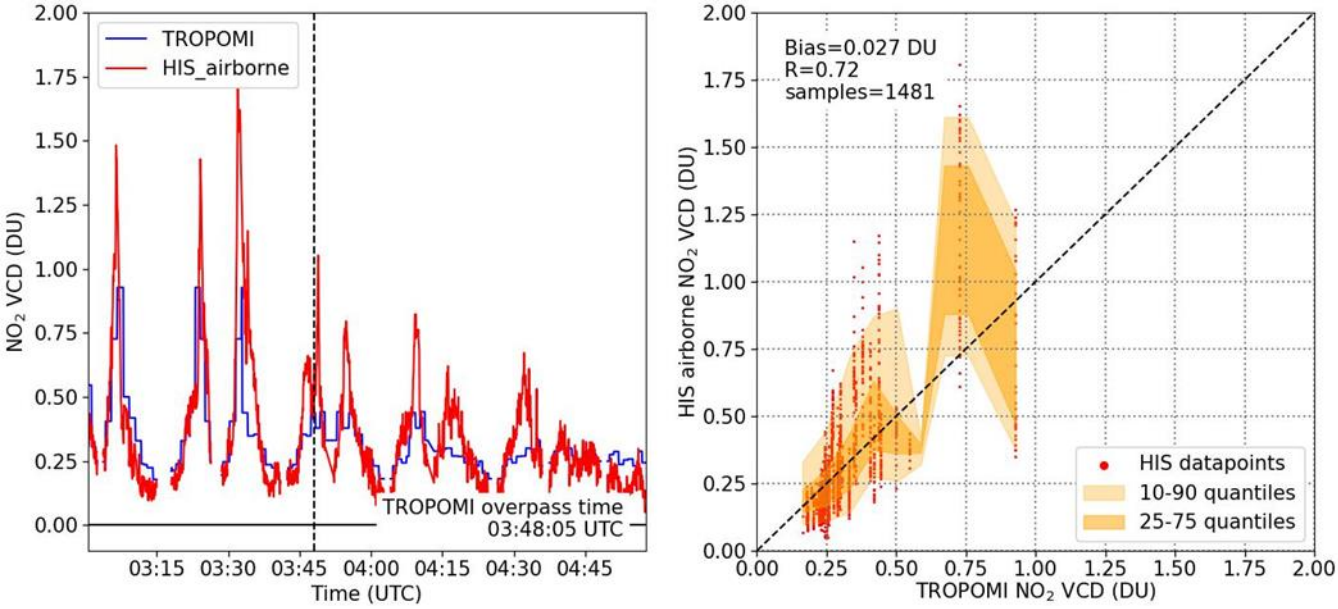

Figure S11. Time series of NO_2 VCD measured from HIS (red line) and TROPOMI (blue line) with TROPOMI overpass time denoted (left) and the scatter plot comparing the HIS and TROPOMI NO_2 VCDs with the corresponding HIS NO_2 VCD quantiles (10, 25, 75, 90th) shown over the TROPOMI NO_2 VCD range (right) for the research flight on 5 November 2020 over the Pohang domain.